Nanosecond Pulse Generation in Optically Pumped Dual-Wavelength Vertical-External-Cavity Surface-Emitting Laser

Zhiwei Li, Jianwei Zhang, Xing Zhang, Zhuo Zhang, Yinli Zhou, Yongqiang Ning, Yugang Zeng, Yue Song, and Lijun Wang

***Abstract*—In this study, nanosecond-pulse lasing was achieved using a vertical-external-cavity surface-emitting laser (VECSEL) with only a single gain chip. A simple linear-cavity setup was used for the VECSEL, and pulsed lasing with a pulse width of ∼9 ns and a repetition frequency of ∼54 MHz was achieved. Dual-wavelength lasing at 974 and 978 nm was observed. The average output power during pulsed operation exceeded 100 mW. As the pumping power was increased, the laser output power could be switched off. However, stable dual-wavelength emission was maintained. The maximum output power under dual-wavelength operation could reach 455 mW.**

***Index Terms*—Pulsed lasing, nanosecond, dual-wavelength, vertical-external-cavity surface-emitting laser.**

I. Introduction

VERTICAL-external-cavity surface-emitting lasers (VECSELs) are compact and versatile laser sources that can offer a high output power, flexible emission wavelength, and diffraction-limited beam quality [1]–[5]. Since the first VECSEL was demonstrated in 1997 [6], this technology has been widely used in the sodium guide star, environment monitoring, laser displays, and medical applications [7]–[10]. Owing to the intrinsic advantages of the external cavity design, VECSEL can be utilized to generate dual wavelength operation by introducing a Fabry–Perot etalon in the cavity [11]–[13]. Although most studies have focused on continuous-wave operations, VECSELs with pulsed operation have been widely reported recently because of their design flexibility and excellent beam quality [14], [15].

Semiconductor saturable absorber mirrors (SESAMs) are always employed to realize pulsed operation of a VECSEL [16], [17]. As the operation of SESAM requires a rather high pumping power density, the beam propagation path within VECSEL should be carefully designed and adjusted [18], [19], and the stability of the entire system should be appropriately maintained. Thus, gain chips with an integrated SESAM structure have been proposed to fulfill the aforementioned requirements. Rudin *et al.* presented a mode-locked integrated external-cavity surface-emitting laser structure [20], which consists of a gain region and a saturable absorber combined into one semiconductor structure. Thus, mode-locking can be achieved in a simple linear cavity. Moreover, two distributed Bragg reflector (DBR) mirror were used in the aforementioned structure to realize optical oscillation of different wavelengths. Recently, Sylvain *et al.* demonstrated the saturable absorbing effect of a single InGaAs quantum well (QW) [21]. As the gain chip was pumped by a mode-locked Ti:sapphire laser, it generated pulsed lasing. In fact, pulsed operation of the gain chip can be realized even without an internal DBR mirror between the gain region and the SESAM. Mahmoud *et al.* reported a SESAM-free VECSEL structure that can generate a stable pulsed signal [22]; this structure is also called the self-mode-locked VECSEL. The Kerr lensing effect inside the VECSEL chip is speculated to be the main reason for the generation of the pulse signal. These methods for pulsed lasing increase the complexity of the optical path and the instability of operation.

Herein, we propose a new method to realize pulsed lasing using a VECSEL with a single gain chip. Two groups of QWs with different band gaps were combined in the active region and were placed next to each other. A pulsed laser beam was generated by the optical absorption and modulation effects of the QWs with narrower band gaps. Dual-wavelength operation was also realized at high pumping powers.

II. Design and Fabrication

A scanning electron microscopy image of the active region of the VECSEL is shown in Fig. 1(a). The active region consisted

Manuscript received December 13, 2021; revised January 28, 2022; accepted February 3, 2022. Date of publication February 8, 2022; date of current version April 22, 2022. This work was supported in part by the National Key Research and Development Program of China under Grant 2018YFB2002401, in part by the National Natural Science Foundation of China under Grants 61874117, 11774343, and 62090060, and in part by Jilin Scientific and Technological Development Program under Grant 20200401006GX. *(Corresponding author: Jianwei Zhang.)*

Zhiwei Li and Zhuo Zhang are with the State Key Laboratory of Luminescence and Application, Changchun Institute of Optics, Fine Mechanics and Physics, Chinese Academy of Sciences, Changchun 130033, China, and also with the Center of Materials Science and Optoelectronics Engineering, University of Chinese Academy of Sciences, Beijing 100049, China (e-mail: lizhiwei17@mails.ucas.ac.cn; zhangzhuo18@mails.ucas.edu.cn).

Jianwei Zhang, Xing Zhang, Yinli Zhou, Yongqiang Ning, Yugang Zeng, Yue Song, and Lijun Wang are with the State Key Laboratory of Luminescence and Application, Changchun Institute of Optics, Fine Mechanics and Physics, Chinese Academy of Sciences, Changchun 130033, China (e-mail: zjw1985@ciomp.ac.cn; zhangx@ciomp.ac.cn; zhouyinli@ciomp.ac.cn; ningyq@ciomp.ac.cn; zengyg@ciomp.ac.cn; songyue@ciomp.ac.cn; wanglj@ciomp.ac.cn).

Digital Object Identifier 10.1109/JPHOT.2022.3149347

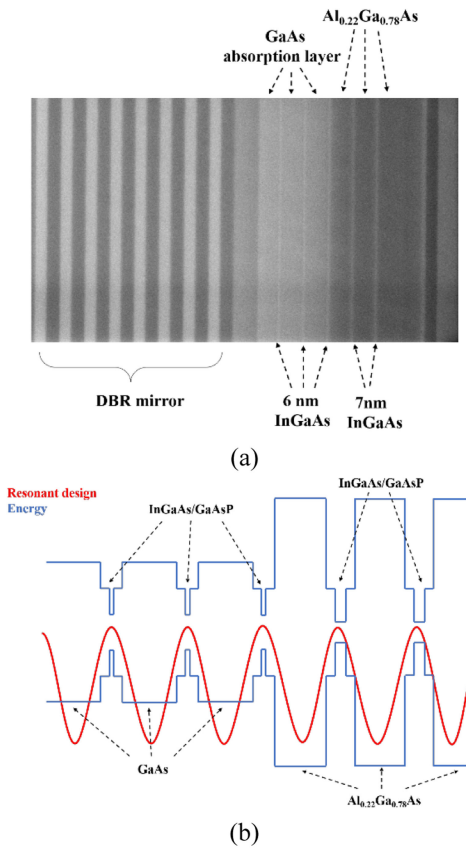

Fig. 1. (a) Scanning electron microscopy image of partial gain chip, whose gain region is composed of two groups of quantum wells with different thicknesses. (b) Energy-band diagrams of active regions in the gain chip.

of two groups of InGaAs QWs. Three 6 nm InGaAs QWs constituted Group 1, and two 7 nm InGaAs QWs constituted Group 2. The In contents of these five QWs were identical. GaAsP barrier layers were used near the QWs to partially compensate for the strain from the QWs. Thus, the emission wavelengths of these two QW groups were slightly different, i.e., ∼975 nm for Group 1 and ∼978 nm for Group 2. Three GaAs absorption layers were inserted near the GaAsP barriers of Group 1, as shown in Fig. 1(b). $Al_{0.22}Ga_{0.78}As$ separating layers were inserted near the GaAsP barriers of Group 2, forming a typical quantum-well-pumped structure. The energy bands of the layers in the active region and the stand-wave distribution are schematically shown in Fig. 1(b). The QWs were placed at the antinodes of the standing wave. The strong optical absorption of the 808 nm pumping laser appeared first in the GaAs absorption layers; thereafter, the QWs of Group 1 facilitated the operation of the VECSEL. As the energy band of the QWs in Group 2 was narrower than that of the Group 1 QWs, the output power of the VECSEL could be modulated by the QWs in Group 2. As the power of the pumping laser was increased, strong in-well pumping was observed for the QWs in Group 2. Thus, dual-wavelength lasing from the QWs in Groups 1 and 2 was observed.

The "bottom emitter" VECSEL structure [23] was utilized in our investigation. The layer structures were grown on a GaAs

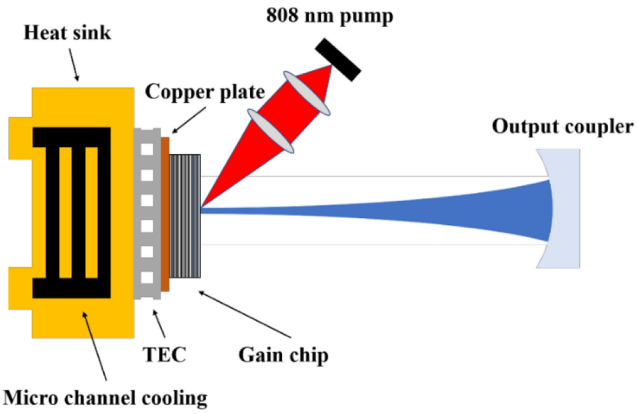

Fig. 2. Schematic of the VECSEL setup.

(001) substrate using a metal organic chemical vapor deposition (MOCVD) AIXTRON 200/4 system. A GaInP etch stop layer was first grown on the substrate. Then, the active region and DBR structure were grown. The DBR structure consisted of 32 pairs of $Al_{0.12}Ga_{0.88}As$/AlAs layers. The center wavelength of the reflectivity spectrum of the DBR was set to 975 nm. After the growth of the epitaxy structure using MOCVD, the wafer was cut into a 3 mm square piece. To maximize thermal management, the epitaxial side was soldered onto a Cu mount. The substrate was removed using selective etching. Then, the etching stop layer was removed, and an anti-reflective mirror was deposited on the gain chip. The other side of the Cu mount was in contact with a copper heat sink, which was cooled using a thermal electric cooler (TEC). The temperature of the heat sink was maintained at 0 °C.

Fig. 2 illustrates the VECSEL laser setup. A linear laser cavity with a single output mirror was used. The total length of the linear cavity was approximately 70 cm. An external mirror with a radius of curvature of 75 mm was used, and its reflectivity was 97% at a wavelength near 975 nm. The gain chip was optically pumped (OP) by an 808 nm fiber-coupled diode laser, and the laser beam was incident on the gain chip at an angle of ∼30°. The pumping laser was coupled with a collimating and focusing system; thus, the beam diameter on the gain chip could be varied to improve the performance of the VECSEL.

III. Results and Discussion

The substrate was removed, and the reflectivity spectrum of the gain chip at 0 °C was measured, as shown in Fig. 3. A flat reflectivity band with a bandwidth of approximately 60 nm was observed. No dips were present in the reflectance, because the noncoherent optical phase was designed to suppress the wavelength selection. Thus, the output wavelength of our VECSEL mainly depends on the position of the gain peak of the QWs.

The photoluminescence (PL) spectra at different pumping powers are shown in Fig. 3 as well. To minimize the influence of the optical reflection of the bottom DBR, the PL spectrum was measured from the edge of the gain chip. Peaks were observed in the PL spectrum. The PL peak at ∼975 nm corresponds to a pumping power of 2.5 W, which indicates the emission

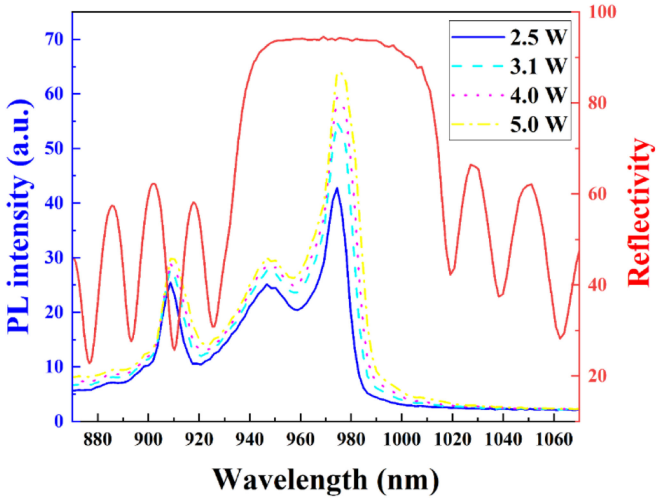

Fig. 3. Measured reflectivity spectrum and photoluminescence spectra of the gain chip under different pumping powers.

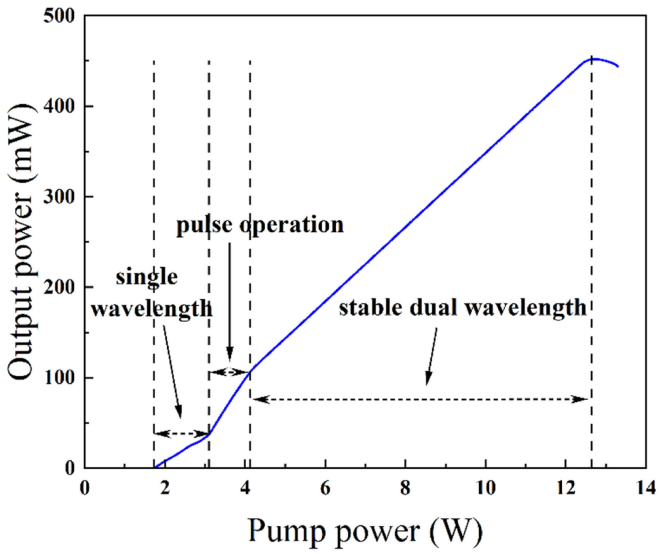

Fig. 4. Output power versus pump power for continuous-wave and pulsed operation.

wavelength of the QWs within the active region. The emission profile becomes broad at higher pumping powers because the QWs in Group 2 get sufficient energy when the pumping power exceeds 3.1 W. Although two groups of QWs were present within the active region, only one peak at ∼975 nm was observed. The main reason for this could be the negligible difference (<5 nm) between the emission peaks of the two QW groups. The PL intensity at the peak near 975 nm increased more rapidly than that at the other peaks when the pumping power was increased. This illustrates the efficient absorption in the active regions on the pumping laser.

The curve of the output power against the incident pump power is shown in Fig. 4. The threshold pumping power was nearly 1.8 W, and the maximum output power of 455 mW was achieved at 0 °C. The maximum average output power during pulsed operation reaches 104 mW. A thermal rollover occurred

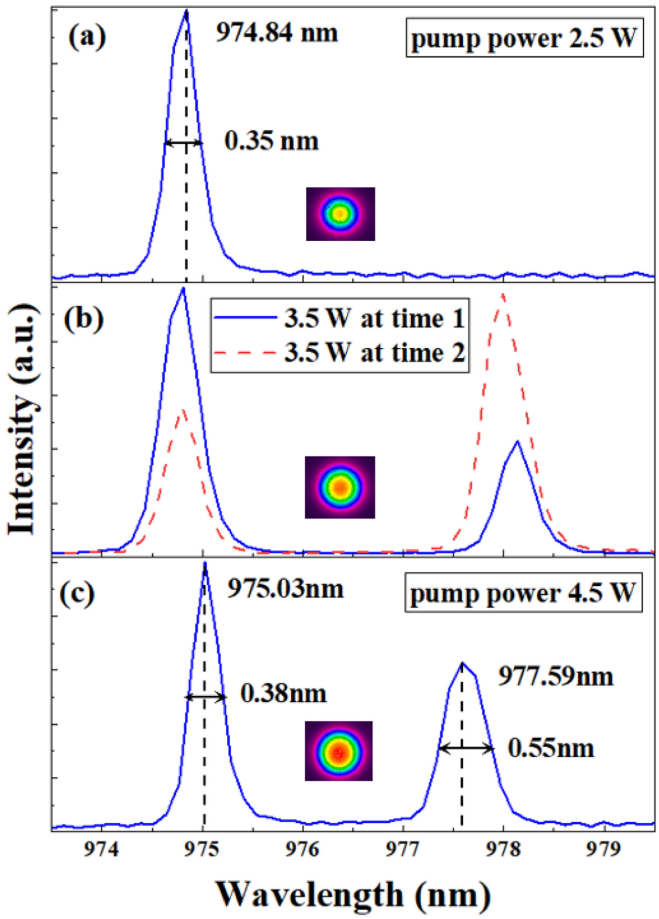

Fig. 5. Emission spectrum of the VECSEL under pump powers of (a) 2.5 W, (b) 3.5 W, and (c) 4.5 W; the beam profiles under different pumping powers are also shown.

when the pumping power was increased further. Two kinks on the power curve can be observed near pumping powers of 3.1 W and 4.1 W. The slope efficiencies of the VECSEL are considerably different before and after reaching the pumping powers corresponding to the kink points.

Fig. 5 shows the emission spectrum of the VECSEL under different pumping powers. As the pumping power exceeds the threshold value, a single lasing wavelength of ∼975 nm can be observed in Fig. 5(a). Although two groups of QWs with different emission wavelengths were present in the active region, only the QWs in Group 1 could offer sufficient optical gain to support laser oscillation. This is because in-well pumping of the QWs in Group 2 requires a high pumping power [24], [25]. However, the QWs in Group 2 could absorb the emission laser generated by the QWs in Group 1; thus, the slope efficiency of the VECSEL under this condition was very low.

As the pump power was increased to 3.1 W, which corresponds to the kink value, dual-wavelength emission was observed, as shown in Fig. 5(b). The emission wavelengths under dual-wavelength operation were ∼975 nm and ∼978 nm, which correspond to the QWs in Groups 1 and 2, respectively. However, the intensities of the two peaks in the spectrum change frequently with time. The intensity of the peak value for each wavelength

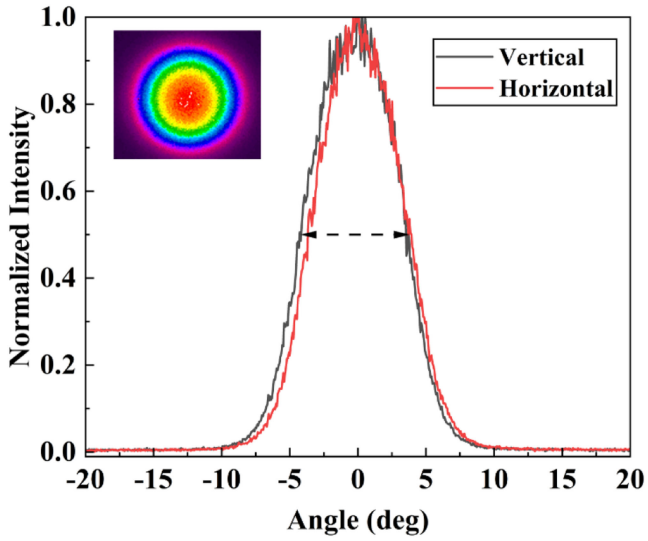

Fig. 6. Far-field distributions of the VECSEL under pumping power of 4.5 W; the inset shows the beam profile.

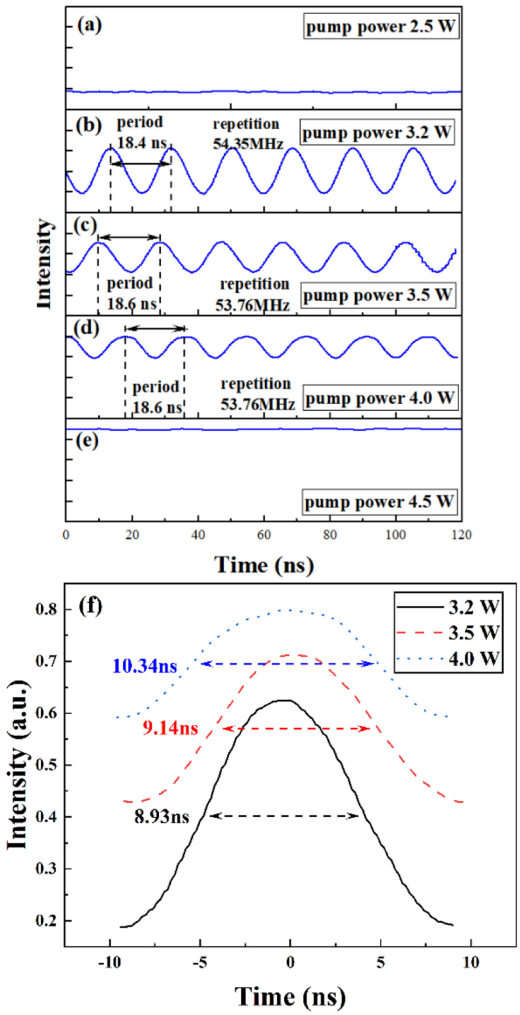

Fig. 7. Pulse shape of the output laser beam from the VECSEL under pumping powers of (a) 2.5 W, (b) 3.2 W, (c) 3.5 W, (d) 4.0 W, and (e) 4.5 W. (f) Enlarged single pulse shapes under different pumping powers.

could be much lower than that of the other. This is very similar to the optical saturated absorption effect [26]–[28]. As the pump power exceeds 3.1 W, the population inversion can be realized in the QWs in Group 2, which absorb light emitted from QWs in Group 1 and then emit laser. As the carrier in QWs in group 2 is exhausted, the QWs in Group 2 can absorb the light emitted from QWs in Group 1 again. This process is repeated, which leads to the intensities of the two peaks in the spectrum to change frequently with time. Thus, the generation of a modulated pulse can be expected during this process. The slope efficiency of the VECSEL under this condition increases due to both Groups of QWs could offer sufficient optical gain to support laser oscillation.

As the pump power exceeded 4.1 W, stable dual-wavelength emission was achieved. The two peak wavelengths were located at 975 nm and 978 nm, and the intensity of the peak value for both wavelengths was not changed with time. The lasing spectra are shown in Fig. 5(c). The peak intensity of the spectrum at 978 nm was slightly lower than that of the spectrum at 975 nm. This is mainly ascribed to the considerably higher carrier density in the QWs in Group 1. As these QWs are surrounded by the absorption layers, they can absorb enough pump light to produce enough photo-generated carriers [29]. A high pump power ensures that the population inversion in the QWs in Group 2 is maintained; thus, the optical modulation of QWs in active region disappears, and the stable dual-wavelength operation can be achieved. The out-beam profiles under different pumping powers were also measured and are shown in Fig. 5. A Gaussian-shaped optical field was observed under different pumping powers. The far-field of the VECSEL pumped at 4.5 W is shown in Fig. 6. The divergence angles of full width at half maximum (FWHM) are 7.74° and 7.59° at two orthogonal directions, and the far fields also show Gaussian cross-sections in both directions.

A biased Si detector was employed to observe the pulsed operation of the VECSEL. The optical beam of the VECSEL was directly collected using the Si detector, which was connected to an oscilloscope. The pulse shapes of the emission lasers under different pump powers are shown in Fig. 6. The VECSEL functioned in the continuous-wave mode under a pumping power of 2.5 W, as shown in Fig. 7(a). Stable pulsed operation was achieved when the pump power was increased from 3.1 W to 4.1 W, as shown in Figs. 7(b)–(d). The pulsed signal started at a pump power of nearly 3.1 W, which corresponds to the previously mentioned kink on the power curve in Fig. 4. Thus, the alternately enhanced intensities of different wavelengths in Fig. 5(b) indicate pulsed operation of the VECSEL. This pulsed operation was enabled by the QWs in Group 2 modulating the optical intensity generated by the QWs in Group 1. The modulation amplitude decreased with increasing pump power, as shown in Figs. 7(b)–(d), main because of the enhanced in-well pumping of the QWs in Group 2. As the pump power was increased, the photogeneration carriers in the QWs in Group 2 also increased. The optical absorption of the QWs in Group 2 was eliminated when the carrier density reached the value of the transparency carrier density of the QWs [30]. Subsequently, non-optical modulation occurred in the gain chip, and pulsed

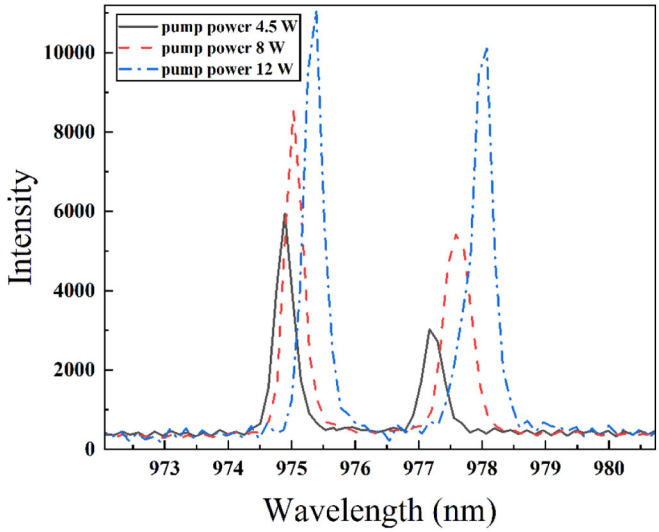

Fig. 8. Dual-wavelength emission spectrum of the VECSEL under different pumping powers.

operation of the VECSEL is switched to continuous wave operation, this can be observed in Fig. 7(e). Therefore, the power slope efficiency of VECSEL decreases when pumping power exceeds 4.1 W which is the terminal power of pulsed operation as shown in Fig. 4. The oscilloscope traces show different baselines because the output power of the laser increases with increasing pump power, and the baseline represents the output power level. In addition, the repetition rate of 54 MHz (period of nearly 18.5 ns) was almost unchanged during the pulsed operation. The pulse characteristics is related to the relaxation time of carriers in QWs. As the pump power has little effect on the carrier relaxation time, the repetition rate is almost unchanged. The QWs in both groups could support stable optical oscillations as the pump power was increased further. Thus, stable dual-wavelength operation could be achieved at higher pump powers, as shown in Fig. 5(c).

The enlarged pulse shapes under the pumping powers of 3.2, 3.5, and 4.0 W are shown in Fig. 7(f). The pulse shape appeared to be highly smooth. A pulse width (full-width half-maximum) of approximately 9 ns was observed. In addition, the pulse widths increased slightly with the pumping power. This is because with increasing pumping power, the carrier concentration increased, which resulted in broadening of the luminescence of the QWs in Group 2; moreover, the thermal effect of increasing the pump power enhanced the exciton scattering [31]. However, the intensity increased as the pumping power was increased further. Thus, the output power of the VECSEL increased as well. The amplitude of the pulse decreased with increasing pumping power, which indicates that the modulation depth of the QWs in Group 2 was reduced. The main reason for this is that the QWs in Group 2 tended to be transparent under strong in-well pumping at a higher pump power [18].

The emission spectra under different pumping powers over 4.1 W are shown in Fig. 8. Stable dual-wavelength emission was achieved when the pumping power exceeded 4.1 W; moreover, the emission wavelengths with a wavelength space of 3 nm were maintained. A slight red-shift of the emission spectrum was also observed due to accumulation of heat in the active region with increasing pump power. Thus, stable dual-wavelength emission could be maintained by the gain chip consisting of two QW groups with different energy bands. The method to realize the VECSEL, which can achieve both dual-wavelength and pulse operation, will be investigated in future research. We believe that the proposed method to generate dual-wavelength emission with pulse modulation would be highly effective in building neural network architectures for computing [32].

IV. Conclusion

To summarize, we demonstrated dual-wavelength and pulsed-operation of an OP-VECSEL comprising a single gain chip and a simple linear cavity. Three different operating mechanisms were observed under different pumping powers. Under pulsed operation, the VECSEL exhibited a ∼9 ns pulse width at a repetition rate of ∼54 MHz. The output power under pulsed operation was more than 100 mW. Stable dual-wavelength operation was also achieved, and a maximum output power of 455 mW was attained. The developed VECSEL with dual-wavelength and nanosecond pulsed operation has considerable potential to be used for creating neural network architectures.

References

[1] K. Nechay *et al.*, "High-Power 760 nm VECSEL based on quantum dot gain mirror," *IEEE J. Quantum Electron.*, vol. 56, no. 4, Aug. 2020, Art. no. 2400404, doi: 10.1109/JQE.2020.2986770.

[2] G.-Y. Hou *et al.*, "High power (>27 W) semiconductor disk laser based on pre-metalized diamond heat-spreader," *IEEE Photon. J.*, vol. 11, no. 2, Apr. 2019, Art. no. 1501908, doi: 10.1109/JPHOT.2019.2908876.

[3] J. Lidan *et al.*, "Frequency doubling of an InGaAs multiple quantum wells semiconductor disk laser," *Superlattices Microstruct.*, vol. 113, pp. 785–790, 2018, doi: 10.1016/j.spmi.2017.12.016.

[4] M. Guina *et al.*, "Optically pumped VECSELs: Review of technology and progress," *J. Phys. D*, vol. 50, no. 38, 2017, Art. no. 383001, doi: 10.1088/1361-6463/aa7bfd.

[5] F. Selmi *et al.*, "Relative refractory period in an excitable semiconductor laser," *Phys. Rev. Lett.*, vol. 112, no. 18, 2014, Art. no. 183902, doi: 10.1103/PhysRevLett.112.183902.

[6] M. Kuznetsov, F. Hakimi, R. Sprague, and A. Mooradian, "High-power (>0.5-W CW) diode-pumped vertical-external-cavity surface-emitting semiconductor lasers with circular TEM00 beams," *IEEE Photon. Technol. Lett.*, vol. 9, no. 8, pp. 1063–1065, Aug. 1997, doi: 10.1109/68.605500.

[7] G. Baili *et al.*, "Experimental demonstration of a tunable dual-frequency semiconductor laser free of relaxation oscillations," *Opt. Lett.*, vol. 34, no. 21, pp. 3421–3423, 2009, doi: 10.1364/OL.34.003421.

[8] J.-Y. Kim *et al.*, "Efficient blue lasers based on gain structure optimizing of vertical-external-cavity surface-emitting laser with second harmonic generation," *J. Appl. Phys.*, vol. 101, no. 3, 2007, Art. no. 033103, doi: 10.1063/1.2432366.

[9] L. Fan *et al.*, "Highly strained InGaAs/GaAs multiwatt vertical-external-cavity surface-emitting laser emitting around 1170 nm," *Appl. Phys. Lett.*, vol. 91, no. 13, 2007, Art. no. 131114, doi: 10.1063/1.2790838.

[10] C. E. Max *et al.*, "Image improvement from a sodium-layer laser guide star adaptive optics system," *Science*, vol. 277, no. 5332, pp. 1649–1652, 1997, doi: 10.1126/science.277.5332.1649.

[11] L. Fan *et al.*, "Linearly polarized dual-wavelength vertical-external-cavity surface-emitting laser," *Appl. Phys. Lett.*, vol. 90, no. 18, 2007, Art. no. 181124, doi: 10.1063/1.2735554.

[12] A. Chernikov *et al.*, "Time-dynamics of the two-color emission from vertical-external-cavity surface-emitting lasers," *Appl. Phys. Lett.*, vol. 100, no. 4, 2012, Art. no. 041114, doi: 10.1063/1.3679607.

[13] M. Scheller *et al.*, "Room temperature continuous wave milliwatt terahertz source," *Opt. Exp.*, vol. 18, no. 26, pp. 27112–27117, 2010, doi: 10.1364/OE.18.027112.
[14] M. Mangold *et al.*, "Femtosecond pulses from a modelocked integrated external-cavity surface emitting laser (MIXSEL)," *Opt. Exp.*, vol. 21, no. 21, pp. 24904–24911, 2013, doi: 10.1364/OE.21.024904.
[15] M. Hoffmann *et al.*, "Femtosecond high-power quantum dot vertical external cavity surface emitting laser," *Opt. Exp.*, vol. 19, no. 9, pp. 8108–8116, 2011, doi: 10.1364/OE.19.008108.
[16] A. Aschwanden *et al.*, "2.1-W picosecond passively mode-locked external-cavity semiconductor laser," *Opt. Lett.*, vol. 30, no. 3, pp. 272–274, 2005, doi: 10.1364/ol.30.000272.
[17] P. Klopp *et al.*, "290-fs pulses from a semiconductor disk laser," *Opt. Exp.*, vol. 16, no. 8, pp. 5770–5775, 2008, doi: 10.1364/oe.16.005770.
[18] U. Keller, "Recent developments in compact ultrafast lasers," *Nature*, vol. 424, no. 6950, pp. 831–838, 2003, doi: 10.1038/nature01938.
[19] U. Keller *et al.*, "Semiconductor saturable absorber mirrors (SESAM's) for femtosecond to nanosecond pulse generation in solid-state lasers," *IEEE J. Sel. Top. Quantum Electron.*, vol. 2, no. 3, pp. 435–453, Sep. 1996, doi: 10.1109/2944.571743.
[20] D. J. H. C. Maas *et al.*, "Vertical integration of ultrafast semiconductor lasers," *Appl. Phys. B*, vol. 88, no. 4, pp. 493–497, 2007, doi: 10.1007/s00340-007-2760-1.
[21] S. Barbay *et al.*, "Excitability in a semiconductor laser with saturable absorber," *Opt. Lett.*, vol. 36, no. 23, pp. 4476–4478, 2011, doi: 10.1364/OL.36.004476.
[22] M. Gaafar *et al.*, "Self-mode-locking semiconductor disk laser," *Opt. Exp.*, vol. 22, no. 23, pp. 28390–28399, 2014, doi: 10.1364/OE.22.028390.
[23] A. C. Tropper and S. Hoogland, "Extended cavity surface-emitting semiconductor lasers," *Prog. Quantum Electron.*, vol. 30, no. 1, pp. 1–43, 2006, doi: 10.1016/j.pquantelec.2005.10.002.
[24] W. Zhang *et al.*, "Operation of an optical in-well-pumped vertical-external-cavity surface-emitting laser," *Appl. Opt.*, vol. 45, no. 29, pp. 7729–7735, 2006, doi: 10.1364/ao.45.007729.
[25] S.-S. Beyertt *et al.*, "Optical in-well pumping of a semiconductor disk laser with high optical efficiency," *IEEE J. Quantum Electron.*, vol. 41, no. 12, pp. 1439–1449, Dec. 2005, doi: 10.1109/JQE.2005.858794.
[26] M. Scheller, C. W. Baker, S. W. Koch, J. V. Moloney, and R. Jason Jones, "High power dual-wavelength VECSEL based on a multiple folded cavity," *IEEE Photon. Technol. Lett.*, vol. 29, no. 10, pp. 790–793, Mar. 2017, doi: 10.1109/LPT.2017.2685595.
[27] F. Zhang, M. Gaafar, C. Möller, W. Stolz, M. Koch, and A. Rahimi-Iman, "Dual-wavelength emission from a serially connected two-chip VECSEL," *IEEE Photon. Technol. Lett.*, vol. 28, no. 8, pp. 927–929, Apr. 2016, doi: 10.1109/LPT.2016.2517702.
[28] M. Wichmann *et al.*, "Antiphase noise dynamics in a dual-wavelength vertical-external-cavity surface-emitting laser," *IEEE Photon. Technol. Lett.*, vol. 27, no. 19, pp. 2039–2042, Oct. 2015, doi: 10.1109/LPT.2015.2449656, doi: 10.1109/LPT.2017.2685595.
[29] S. B. Morioka, "High-power optically pumped semiconductor laser applications," in *Proc. SPIE Conf. Vertical External Cavity Surf. Emitting Lasers*, vol. 7919, 2011, Art. no. 791913.
[30] Y. F. Chen *et al.*, "Femtosecond high-power spontaneous mode-locked operation in vertical-external cavity surface-emitting laser with gigahertz oscillation," *Opt. Lett.*, vol. 36, no. 23, pp. 4581–4583, 2011, doi: 10.1364/OL.36.004581.
[31] D. Vashaee and A. Shakouri, "Electronic and thermoelectric transport in semiconductor and metallic superlattices," *J. Appl. Phys.*, vol. 95, no. 3, pp. 1233–1245, Jan. 2004, doi: 10.1063/1.1635992.
[32] W. Maass *et al.*, "Real-time computing without stable states: A new framework for neural computation based on perturbations," *Neural Comput.*, vol. 14, no. 11, pp. 2531–2560, Nov. 2002, doi: 10.1162/089976602760407955.